

Article

Fluid-Structure Interaction Analyses for Hydro-Elastic Tailoring of a Windsurfer Fin

Miguel Cardoso de Brito ¹, Leigh Stuart Sutherland ^{2,*} , José Manuel C. Pereira ³ and Mário Rui Arruda ⁴ 

¹ Department of Mechanical Engineering (DEM), Instituto Superior Técnico, Universidade de Lisboa, 1049-001 Lisbon, Portugal

² Centre for Marine Technology and Ocean Engineering (CENTEC), Instituto Superior Técnico, Universidade de Lisboa, 1049-001 Lisbon, Portugal

³ Associated Laboratory for Energy, Transports and Aeronautics (LAETA, IDMEC), Instituto Superior Técnico, Universidade de Lisboa, 1049-001 Lisbon, Portugal

⁴ Civil Engineering Research and Innovation for Sustainability (CERIS), Instituto Superior Técnico, Universidade de Lisboa, 1649-001 Lisbon, Portugal

* Correspondence: l.sutherland@tecnico.ulisboa.pt

Abstract: A fully iterative ‘two-way’ fluid-structure interaction (FSI) tool of a commercially available composite windsurfer fin was developed, which was then used to investigate the normally hidden fin behaviour for a range of typical sailing conditions. The ‘two-way’ FSI analysis gave significantly better insights into the fin behaviour than the simpler ‘one-way’ non-iterative analysis. The tool also indicated that hydro-elastic tailoring, via simple reinforcement ply rotations, can produce large changes in tip twist. This gives an opportunity for both improved passive control and higher speeds, without deviating from a hydrodynamically optimal plan form. Inexpensive cantilever tests appear to be sufficient to make qualitative comparisons between the sailing responses of fins with different layups.

Keywords: fluid-structure interaction; hydrofoils; sailing; marine composites; hydro-elastic tailoring



Citation: Cardoso de Brito, M.; Sutherland, L.S.; Pereira, J.M.C.; Arruda, M.R. Fluid-Structure Interaction Analyses for Hydro-Elastic Tailoring of a Windsurfer Fin. *J. Mar. Sci. Eng.* **2022**, *10*, 1371. <https://doi.org/10.3390/jmse10101371>

Academic Editors: Vincenzo Crupi and Giulia Palomba

Received: 8 August 2022

Accepted: 16 September 2022

Published: 26 September 2022

Publisher’s Note: MDPI stays neutral with regard to jurisdictional claims in published maps and institutional affiliations.



Copyright: © 2022 by the authors. Licensee MDPI, Basel, Switzerland. This article is an open access article distributed under the terms and conditions of the Creative Commons Attribution (CC BY) license (<https://creativecommons.org/licenses/by/4.0/>).

1. Introduction

Windsurfing is a relatively new sailing sport (with roots in the early 1960s [1]) which has rapidly developed equipment capable of extremely high sailing speeds (over 50 knots [2]) and has now become an Olympic sport. The innovative application of advanced fibre composites has been central to this development, and the sport has always been at the vanguard of the introduction of such materials (e.g., carbon fibre foils and spars, ultra-lightweight sandwich construction and novel sail materials) into the wider marine industry.

The fin, or ‘foil’, is equally as important as the other two constituent parts of a windsurfer—the ‘rig’ (sail, boom and mast) and the board. In fact, the fin can be viewed as the mirror image of the rig, whose lateral side force it is designed to oppose [3,4], the marked size difference between the fin and rig (as hydrofoil and aerofoil, respectively) simply a consequence of the disparity between the densities of air and water. As the wind strength increases the sailor will need to select a smaller sail from their ‘quiver’ of sails, and due to the requirement for hydro-aerodynamic balance will simultaneously select a correspondingly smaller fin. Further, since more challenging conditions (in terms of sea-state and/or wind strength and/or stability) require more control from the fin, the sailor will often also have the choice of a selection of different fin types.

The driving force of high-level competition very quickly evolved fin design from the early simple un-reinforced plastic ‘skegs’ into the current high-performance carbon-composite ‘lateral hydrofoils’ with highly efficient foil sections and planforms. This evolution has resulted in various basic fin designs, each with attributes fitting the ‘niche’ of the intended sailing discipline—from control-biased wave sailing, through slalom, to speed-biased course racing. Control is usually achieved via ‘twist-off’ (wash-out) at the fin

tip to progressively reduce angles of attack at high loadings, and is normally realised via aft-swept planforms and aft rake to give the typical ‘dolphin fin’ shape of the wave fin. The hydrodynamically more efficient upright course racing fins with elliptical planforms result in better lift to drag ratios at the expense of more sudden, and hence uncontrollable, stall behaviour. Slalom fins tend to aim at a compromise between these two extremes.

The importance of the fin in terms of the overall hydro-aerodynamic force balance means that a professional, or even fairly accomplished, sailor can immediately and acutely feel the effects of even apparently very small changes to the fin design. In fact, despite some scientific interest in the subject, mostly in the 1990s [3–11], the development of modern fins has been achieved via empirical ‘on-the-water’ testing of new ideas, facilitated by the fact that as a small component, prototypes are relatively easily fabricated. This approach is perhaps not surprising given the complexity of the problem in terms of fluid flow, complex anisotropic composite structural deformations and the hydro-elastic interaction between the two, which has made this empirical approach far more attractive, productive and certainly economical than comprehensive mathematical modelling attempts.

However, this has led to a situation where whilst it is generally known which fin designs give good results, it is not exactly known why. There are many, and often anecdotal, theories within the windsurfing community, based to a greater or lesser degree on the perceived physics of the problem, but these are very difficult to prove or otherwise given that it is not easy to see how the fin actually responds to the water flow under the board. Hence, the current work develops a design tool using modern fluid structure interaction (FSI) hydro-elastic numerical analyses in Section 2, which is then used to investigate the expected response of the fin to a range of typical sailing conditions in Section 3, thus starting to ‘de-mystify’ the mechanisms behind the performances of different fin designs.

Such a tool would also then be invaluable in the design of improved performance fins, allowing preliminary investigation of different designs before selecting a small number of candidate fins for manufacture and (still essential) final on-the-water testing. An important advantage of fibre composite materials is that the lay-up may be tailored to the loading paths, and this has already been achieved by the industry with the use of unidirectional (UD) plies to take the main cantilever type loadings, and of $\pm 45^\circ$ bidirectional plies to resist twisting moments. However, this aspect could be further exploited via hydro-elastic tailoring of the lay-up to encourage passive control twist, thus removing the dependency of twist characteristics on the planform shape and allowing the design of a ‘best of both worlds’ high lift to drag ratio upright fin with the high control of a swept-back wave fin (see Section 4).

Finally, the windsurfing fin is simply a hydrofoil at 90° to the water surface, and hence any studies of it are relevant to other types of hydrofoil with different orientations. The inexorable advance of the ‘foiling revolution’ throughout the various water sports communities is no overstatement. Nowadays, all manner of craft from surfboards, through sailing dinghies, production yachts and America’s Cup boats, to large circumnavigating ‘speed machines’ are now flying above the water surface at previously almost unimaginable sailing velocities. This has only been made possible with the use of extremely high specific stiffness carbon composites. Similarly, the blades of composite tidal turbines, and ship and motor-boat propellers are, of course, all rotating foils.

2. Numerical Model

2.1. Structural Analysis

The first step towards developing the design tool was to build a structural model in order to be able to assess the fin’s behaviour under hydrodynamic loading.

2.1.1. Geometry and Lay-Up

This study concerns an actual production fin, a 37 cm Slalom fin manufactured by F-Hot fins Ltd. (Colchester, UK), a leading supplier to world class competitive sailors, the planform and proprietary section geometries of which are shown in Figure 1.

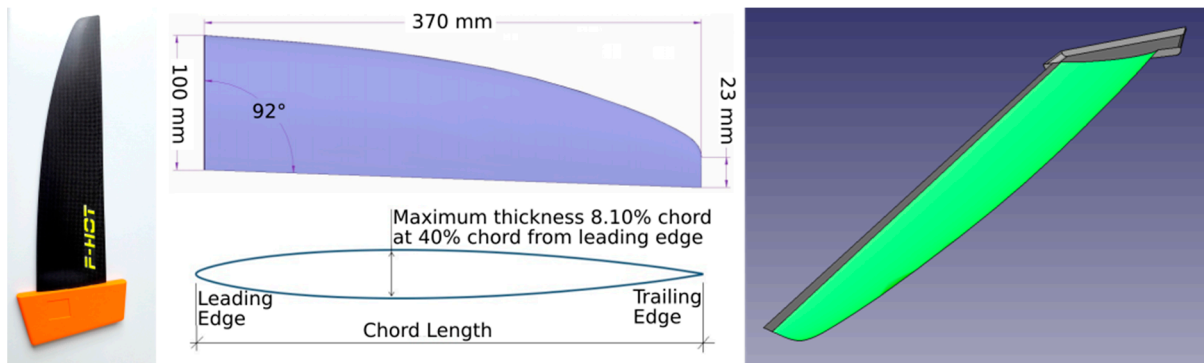


Figure 1. Slalom fin (and mould) geometry.

The port and starboard side plies are hand laid up using epoxy resin separately in a split female aluminium mould, and after application of a thin layer of epoxy/carbon short fibre paste to fill any central voids, the two flanged sides of the mould are bolted together. The fin is then left to cure as a single piece at 50 °C for 24 h. The exact layup schedule is commercially sensitive information, but each side consists of 5 full face outer layers of $\pm 45^\circ$ bi-directional and 0° UD carbon, followed by 9 and 5 plies of 0° UD carbon and E-glass tapes, respectively (where ply angles are defined with respect to the trailing edge). These tapes vary in width and length from 50 to 70 mm, and from 140 to 240 mm, respectively.

The structural numerical model of the fin used the ABAQUS finite element analysis (FEA) software [12]. The fin input geometry was taken from the IGES files used for the CNC production of the two mould halves, which were then combined using Rhino CAD software [13] into a single geometry input file. Thickness measurements taken over the surface of an actual fin supplied by the manufacturer confirmed the accuracy of this geometry input file. In order to define the varying internal ply structure, and to allow meshing of the model, the fin's 3D internal space was partitioned into various segments corresponding to areas of the fin with specific numbers of plies (Figure 2).

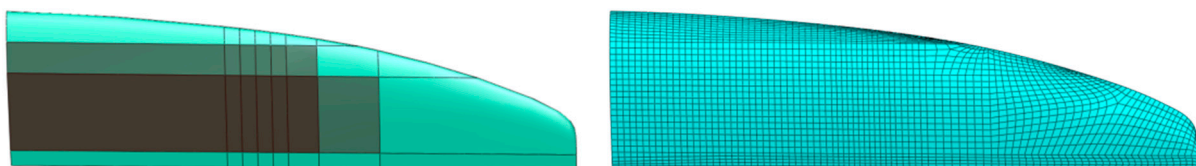


Figure 2. FEA Partitions (shaded areas = UD tapes) and mesh.

2.1.2. Elements, Mesh and Boundary Conditions

Shell elements were preferred over solid elements to model more precisely the complex fin geometry, and to reduce computational expenses. However, a continuum shell element was used since conventional shell elements would not be capable of defining the inner epoxy/carbon paste filled volumes with geometrical thickness. Specifically, the SC8R general-purpose, 8-node, hexahedral, first-order, reduced-integration, continuum shell element was used. This element accounts for finite membrane strains, arbitrary large rotation, and allows for changes in thickness, making it suitable for this large-strain/displacement analysis [14].

The various composite layups in each partition of Figure 2 were defined as ABAQUS 'composite sets' since this allows the laminate mesh to subdivide through the laminate thickness.

The SC8R element required hexahedral meshing, and since it is a first-order reduced-integration element, 'hour-glassing' (where elements distort uncontrollably in such a way that the strains calculated at the integration point are all zero [15]) must be avoided by making the mesh sufficiently fine. Therefore, the linear hourglass control option was also enabled.

A nominal global mesh size of 4 mm was selected via a mesh sensitivity study, resulting in 13,824 elements. As can be seen in Figure 2, zones of mesh refinement were introduced at the leading and trailing edges due to the increased curvature in these areas.

The fin is mounted into the bottom of the board via a male wedge-shaped ‘head’ (in orange in the photo of Figure 1) that is pulled very tightly into a reciprocal female wedge-shaped ‘fin box’ embedded into the board. A vertical bolt passing through the board into a threaded bolt embedded in the fin head pulls it up into the fin box giving a very tight fit. This arrangement, together with lateral ‘floors’ which reinforce the fin box against rotations within the board, result in an extremely stiff cantilever type mounting arrangement. Hence, the base of the FEA modelled fin foil section was restricted here with boundary conditions preventing both translation and rotations in all directions.

As further detailed in Section 2.1.3, for validation of the structural model, single point loads were applied to one side of the fin only. For the FSI analyses of Section 2.3 the pressure loadings on both faces obtained from the CFD model were applied.

2.1.3. Material Properties and Structural Model Verification

As is common for marine composites, the materials used here are not the well-documented and regulated factory impregnated ‘pre-pregs’ as used within the aerospace industry, and so material properties may not be simply obtained from laminate data sheets. In fact, due to the small scale of this particular sector of the marine industry, these fins are hand laid up and there are no (expensive) material properties testing programmes. Hence, not only are there no available material properties data, but also the estimation of them is hampered by a lack of information on the ratio of fibres to resin, the fibre volume fraction (FVF), in the finished laminate, which is required to estimate them. Hence, the engineering approach described below was developed.

The laminator (with 40 years of experience) categorised the layup as one with a higher-than-normal resin ratio to ensure durability of the fins to impacts. Measurements of the weights of fibres and resin used in the manufacture of a fin were taken, giving an FVF estimate of 0.4 from the known densities of the materials used, which corresponded with the lower ranges of FVF for hand laid up marine composites to be found in the literature [16,17].

Next, knowing the fibres and resin used in the fin, experimentally obtained library elastic material property values (Young’s Modulus, E , Poisson’s Ratio, ν and Shear modulus, G ; each in all three orthotropic directions) for equivalent hand laid up woven and UD carbon, and UD E-glass were obtained from the material property library of another FEA software, ANSYS (Canonsburg, PA, USA) [18]. However, these library values were for laminates of higher FVF (from 0.5 to 0.65) than of those considered here (0.4) and so these library properties were adjusted for these differences in FVF using the generalised rule of mixtures (ROM) equations [19]. For example, for longitudinal stiffness, E_1 , for two laminates ‘A’ and ‘B’ equivalent in all respects except for FVF (V_f):

$$E_{1,c} = \eta_0 \eta_L E_{1,f} V_f + E_m (1 - V_f) \tag{1}$$

and

$$E_{1,c,B} = \frac{\eta_0 \eta_L E_{1,f} V_{f,B} + E_m (1 - V_{f,B})}{\eta_0 \eta_L E_{1,f} V_{f,A} + E_m (1 - V_{f,A})} \times E_{1,c,A} \tag{2}$$

where the subscripts c, f and m refer to composite, fibre and matrix resin, respectively, and $\eta_0 = 1.0$ for UD and 0.5 for woven reinforcements, and $\eta_L = 1.0$ (since fibre lengths > 10 mm).

This semi-empirical approach, rather than direct ROM estimation of the material properties directly from the fibre and resin properties, was used since the use of experimentally obtained base values ensured that irregularities introduced via hand lay-up and other factors not considered by ROM were inherently included.

These values were then verified using a corresponding set calculated using the Chamis set of semi-empirical equations [20–22] directly from the resin and fibre material properties

and a typical hand lay-up void fraction of 0.05 [23,24]. This gave values very close to the previously calculated ‘ROM adjusted FVF’ data in all cases, thus increasing confidence in the material property input data.

To verify the FEA model, experimental force-deflection data from a simple cantilever loading of the fabricated fin was used. Two-point loading cases, both at $\frac{1}{4}$ chord from the leading edge, were performed; one at 40% and one at 80% span from the fin base [25] (Figure 3). These two different cases with differing ratios of shear and bending influence, allowed a more rigorous validation of the FEA model. A calibrated, displacement-controlled servo-hydraulic test rig with load cell and displacement transducer outputs was used for these tests.

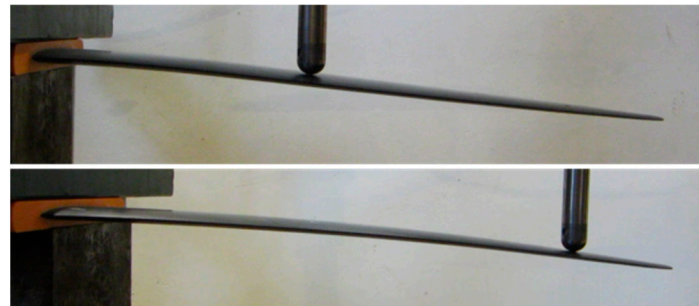


Figure 3. Experimental fin tests [24].

After further discussions with the manufacturer and observations of the lamination process, it was noted that the plies were not laid up in the mould with the fibres exactly straight along the fin span but were curved to some degree. This occurred due both to natural fibre movements during the rolling stage of hand layup, and to the need to fit the plies into the mould with its curved leading edge plan shape. Even a slight curvature of the plies in the laminate is known to decrease the stiffness in the fibre direction [25]. Measurements of the fibres in the plies as they were laminated estimated this fibre ‘waviness’ to be of the order of 2.5 mm amplitude in a wavelength of 10 cm, giving a Young’s modulus reduction of a factor of 0.25 according to [26] (in their). This reduction was applied to all UD and woven longitudinal and woven transverse Young’s modulus, E , values, resulting in the material properties given in Table 1.

Table 1. Ply material properties.

	UD Epoxy/e-Glass	UD Epoxy/Carbon	Woven Epoxy/Carbon
E_1 (Pa)	2.23×10^{10}	5.66×10^{10}	2.84×10^{10}
E_2 (Pa)	7.90×10^9	5.11×10^9	2.84×10^{10}
E_3 (Pa)	7.90×10^9	5.11×10^9	5.54×10^9
ν_{12}	0.29	0.31	0.04
ν_{23}	0.40	0.42	0.30
ν_{13}	0.29	0.31	0.30
G_{12} (Pa)	4.12×10^9	3.26×10^9	3.30×10^9
G_{23} (Pa)	3.50×10^9	3.08×10^9	2.70×10^9
G_{13} (Pa)	4.12×10^9	3.26×10^9	2.70×10^9

Using these material properties inputs (derived via careful consideration of the actual fabrication process used rather than simply via ‘calibration’ to fit the numerical to the experimental results) for the FEA model resulted in very good predictions of the fin experimental test values (Figure 4), especially given the inherent variability of the hand layup process used, thus providing a validation of the numerical structural model. The small variation between numerical and experimental results, together with this inherent variability and the unavoidable experimental errors, do not allow any confident interpretation of the fact

that the 40% and 80% span experimental results are stiffer and more flexible than the FEA predictions, respectively.

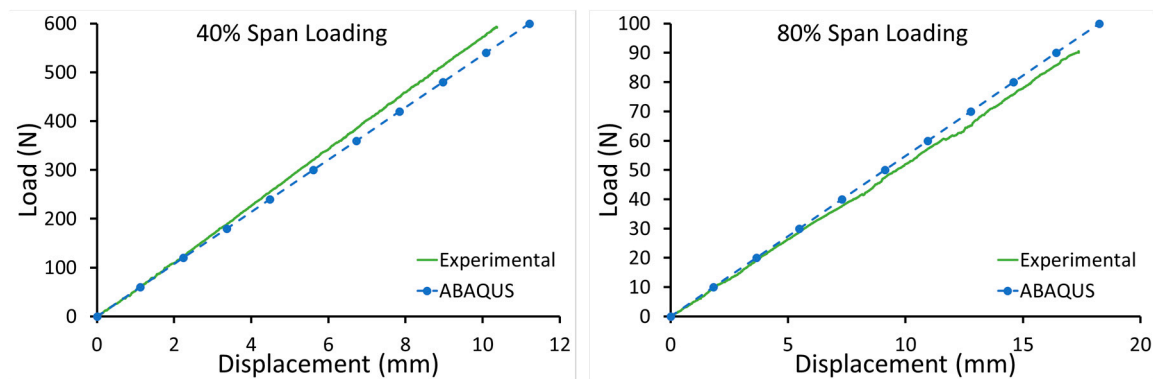


Figure 4. Comparison of ABAQUS FEA structural model and cantilever fin test results.

2.2. Computational Fluid Dynamics Analysis

The analyses performed here used a previous study as a starting point [27], and uses Star-CCM+ [28] since this software can both analyse accurately turbulent fluid flow around wing shaped geometries [29], and also integrates seamlessly with ABAQUS FEA software for FSI analyses. The same geometric model as used in this study for the FEA was used, with just the very leading edge needing to be slightly rounded in order to eliminate numerical singularities in the CFD analysis. However, this extremely localised geometry change would not affect the FEA results.

A simple rectangular prism fluid domain (of dimensions $16 \times 10 \times 8$ fin base chord lengths, respectively) with the fin base located on the upper face (centred laterally, 6 base chord lengths from the inlet face) was constructed (Figure 5a). The boundary condition types assigned were 'Wall' for the fin surface, 'Pressure Outlet' for the outlet aft face, and finally 'Velocity Inlet' for the inlet, lateral faces and bottom face, where there are unperturbed flow conditions. In practice, the fin base is inserted into the flat underside of the board, which would hence cover part of the upper face of the fluid domain. However, since the boundary layer at the board is less than 1 cm thick and after confirmatory tests to ensure that this would not affect results, the board was not modelled and the whole upper face was modelled as a 'Velocity Slip Wall'; forcing zero vertical velocities to represent the water-air interface and hence significantly reducing computational time and complexity. The 'Velocity Inlet' flows were assigned to give the required angle of attack to the fin in each case.

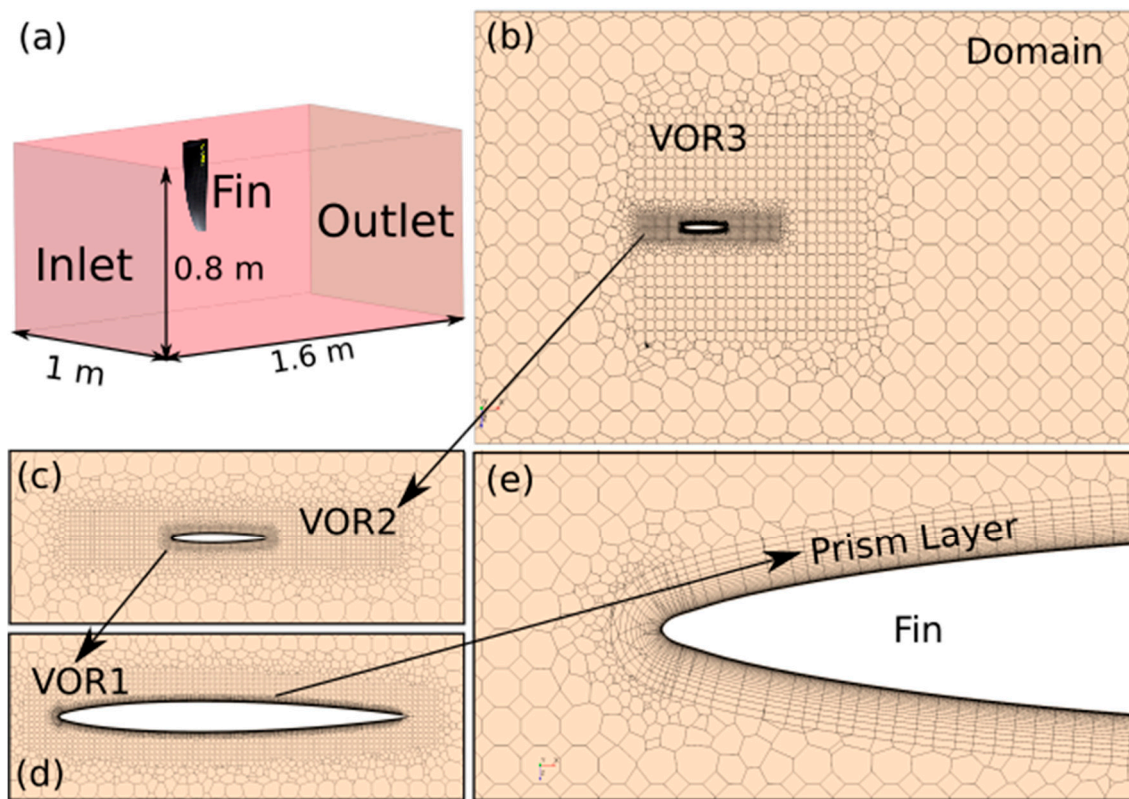


Figure 5. Computational fluid domain (a), boundary surfaces and mesh refinements (b–e).

The ‘Automated Mesh’ feature of Star-CCM+ was used to mesh the domain, with increasingly fine volumes of refinement (VORs) from the outer domain to the fin surface (Figure 5b–d) to accurately model the flow whilst saving computational expense. Since the analysis of the flow of the boundary layer is especially important, a prism layer that closely followed the fin profile was used next to the fin surface (Figure 5e). ‘Surface Remesher’, ‘Polyhedral Mesher’ and ‘Prism Layer Mesher’ were used for the fin surface, VORs and prism layers, respectively. The mesh parameters used are given in Table 2.

Table 2. Mesh parameters.

Base size	50 mm
Domain relative cell size	150%
VOR 3 relative cell size	50%
VOR 2 relative cell size	10%
VOR 1 relative cell size	3%
Number of prism layers	25
Prism layer thickness	2 mm
Prism layer stretching	1.17
Wall y^+	≈ 1
Number of xells	$\approx 3 \times 10^6$

The following physical continuum models were chosen for all CFD simulations [27]:

- Three-dimensional analysis
- Steady and segregated flow
- Constant density
- Turbulent flow solving the Reynolds-averaged Navier–Stokes equations
- $K-\omega$, SST (menter) turbulence model
- $\gamma-Re_\theta$ transition model
- Low y^+ wall treatment

The fluid assumed for all simulations was 35 g/kg salinity seawater at 20 °C, of density (ρ) 1024.9 kg/m³ and dynamic viscosity (μ) 1.077×10^{-3} Pa·s [30]. Residuals convergence criteria (at 10^{-4}) were used to give solutions that required around 180 computational hours each running in 18 parallel cores, giving a wall time of 10 h.

2.3. FSI Analysis

The extremely light and stiff carbon composite construction of windsurfing fins has allowed the fabrication of foils with hydrodynamically efficient fine chord profiles that would not be possible with other economically viable material systems. However, these fins are subject to extremely high loads and deflections can be very large, and hence a simple 'one-way' analysis (where CFD loads assuming a completely rigid fin are applied once to the structural model to give the structural response) may well not be sufficient in all cases. A full 'two-way' iterative FSI, analysis that then takes this first deformed geometry and re-evaluates the CFD loadings for iterative re-application to the structural model until convergence is achieved, will more closely model such a hydro-elastic case. However, a one-way FSI will be far less expensive (both computationally and in terms of technical resources, time and finances) which is critical for the typically very small fin producer, as well as for the huge majority of other marine composite fabricators. Hence, it is important to know when and where the simpler one-way FSI may be safely used with sufficient accuracy, over the full two-way analysis.

The FEA and CFD models of Sections 2.1 and 2.2 were connected via the Simulia Co-Simulation Engine (CSE), which enables fully automatic communication between the two for import and export of field properties and mesh information. The CSE required that the same fin surface was present and with the same name in both CFD and FEA solvers. In this region, displacements are exported from FEA to CFD solvers, and pressures and wall shear stresses exported in the opposite direction [15]. The lack of a prescribed unit system in ABAQUS requires that special care be taken to ensure that the same units are used in both solvers.

Since fin deflections were expected to be significant, an iterative dynamic implicit approach was used, where fields are exchanged multiple times per coupling step until an overall equilibrium is achieved prior to advancing to the next step. This iterative coupling scheme allows one analysis to lead, which (as is highly recommended [31]) was the structural (ABAQUS) solver. A constant coupling step size of 0.1 s for both FEA and CFD solvers, allowing both analyses to advance in parallel, was used after tentative experimentation (guided by previous experience) showed this value to give good solution convergence for the present steady-state problem. Especially for operating conditions with higher fin deflections and pressures, and at the start of each simulation, ramping of the pressure field was also required for solution convergence. The same residual convergence criteria used for the CFD analysis (Section 2.2) were also used for the FSI analyses.

3. Parametric Study

The behaviour of the fin under a range of typical sailing conditions was next investigated using the developed FSI analysis tool. These conditions may be represented by combinations of two main parameters, velocity and angle of attack (AoA). To bypass the extremely complex task of identifying the specific velocity and AoA on all points of sailing for all of the possible weather and sea states, a parametric study of all permutations of a range of sensible velocities and AoAs was completed. The CFD analysis indicated that stall occurred at around 8° AoA, and a reasonably typical upper velocity limit of 35 knots was assumed. Hence, a test matrix of five levels of velocity (10, 15, 20, 25, 30 and 35 kn) at three levels of AoA (2, 4 and 6°) was studied.

Multiple fin responses must be considered to describe fully fin behaviour under different sailing conditions. Aero-hydrofoil theory and the accumulated empirical conclusions of decades of the sport have led to the conclusions that (a) 'lift' (in the lateral, opposing sail side force sense) and drag forces, and (b) twist (thus varying the local tip AoA) and

tip (cantilever) deflection, are important in terms of performance and control, respectively. Hence, this parametric study investigates these four responses.

Further, a two-way FSI may well produce more refined results than a one-way FSI (especially as the fin is increasingly ‘loaded up’ at higher velocities and/or AoAs, and deflections increase), but this will come at considerably increased cost, time, software and expertise requirements that may well be prohibitive for the windsurfing industry. Conversely, since just a single computation of the pressure field over the fin is required for the one-way FSI, this may be an affordable option, if its accuracy is acceptable. Hence, under exactly which conditions, and for which fin responses, the advantages of a more expensive two-way FSI over a one-way FSI are not significant was also investigated.

3.1. Results

The results of the parametric study in terms of the responses lift force, drag force, tip twist and tip deflection are shown in Figures 6–9, respectively.

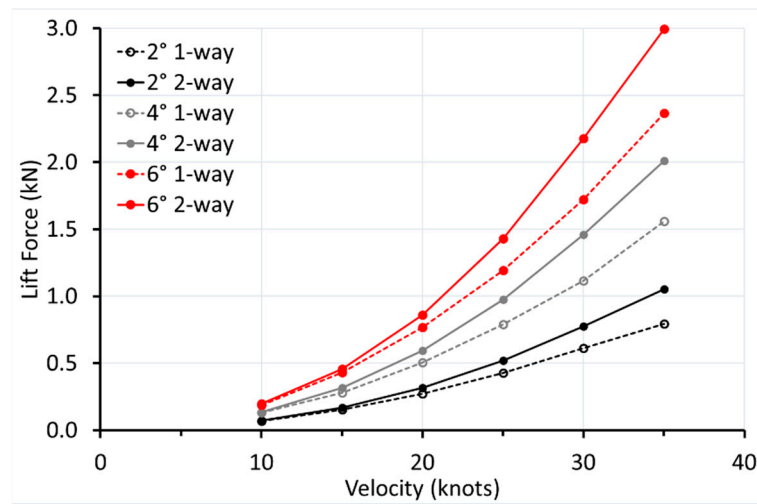


Figure 6. Lift force vs. velocity.

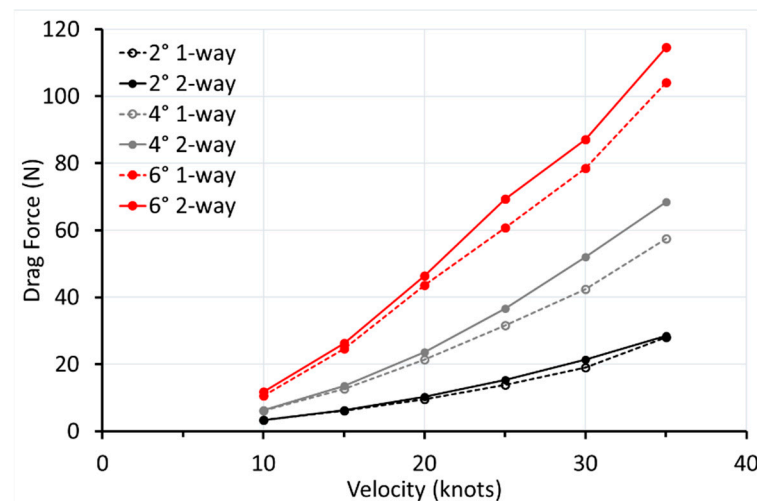


Figure 7. Drag force vs. velocity.

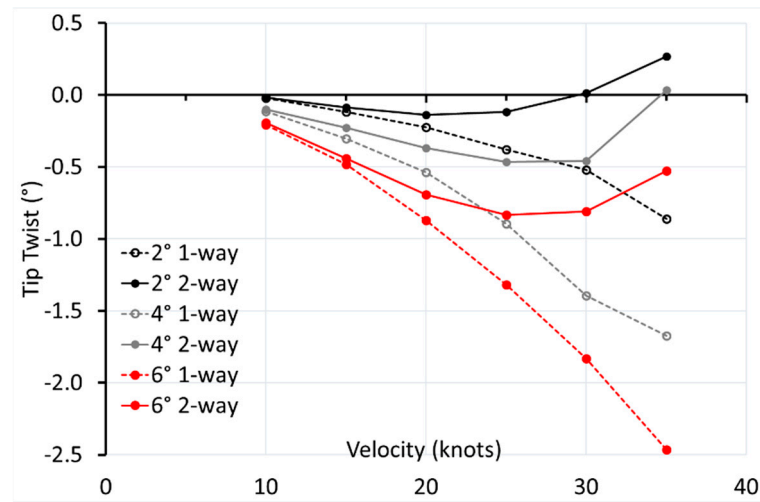


Figure 8. Tip twist (negative = wash-in = increased AoA) vs. velocity.

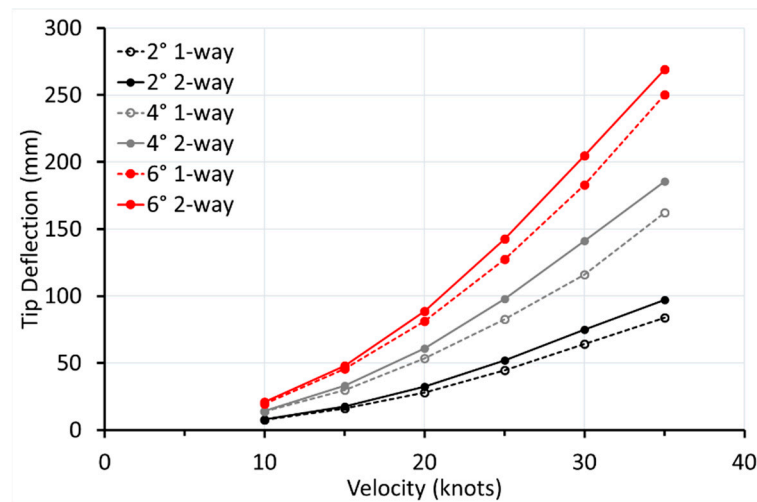


Figure 9. Tip deflection vs. velocity.

3.2. Discussion

It is important to remember in the context of the discussions below that the CFD derived loads in the one-way and two-way analyses assume the un-deformed and deformed fin geometries, respectively.

3.2.1. Lift

As expected, Figure 6 shows lift force increasing with velocity and (base chord) AoA, for both one-way and two-way analyses. It is also clear from Figure 6 that the two-way analysis predicts more lift force than does the one-way analysis, and that this difference increases monotonically with velocity. The tip wash-in (increased AoA) predicted by the two-way analysis for most cases (Figure 8) could account for some increase in lift force over that predicted by the one-way analysis (which assumes an un-deformed fin with zero wash-in). However, this figure, together with Figure 10, show that this does not fully explain the higher two-way predicted loads since lift force continues to increase even as tip twist drops off at the highest velocities for the two-way analysis.

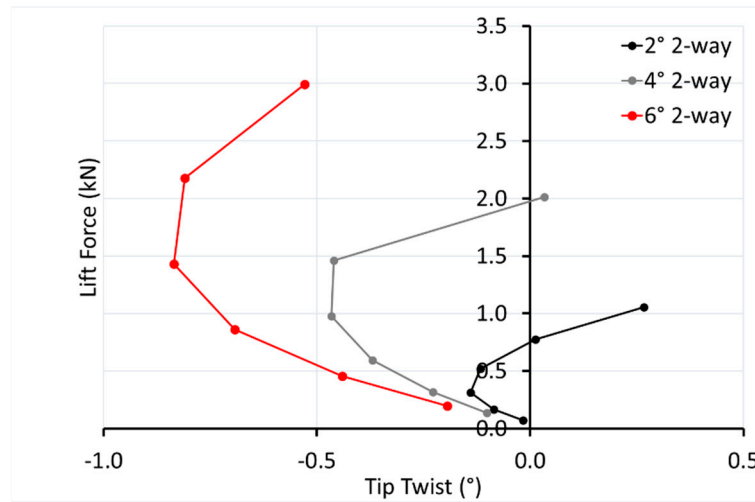


Figure 10. Lift force vs. tip twist.

For the one-way analysis, the lift coefficient, C_L in Equation (3), is relatively constant with increasing Reynold’s number, Re , (Figure 11), as might be expected from classical aerofoil theory, and the fact that the CFD of the one-way analysis only considers the un-deformed fin geometry.

$$C_L = \frac{2L}{\rho v^2 A} \tag{3}$$

where L is lift force, ρ fluid density, v the flow speed and A the surface area of the fin.

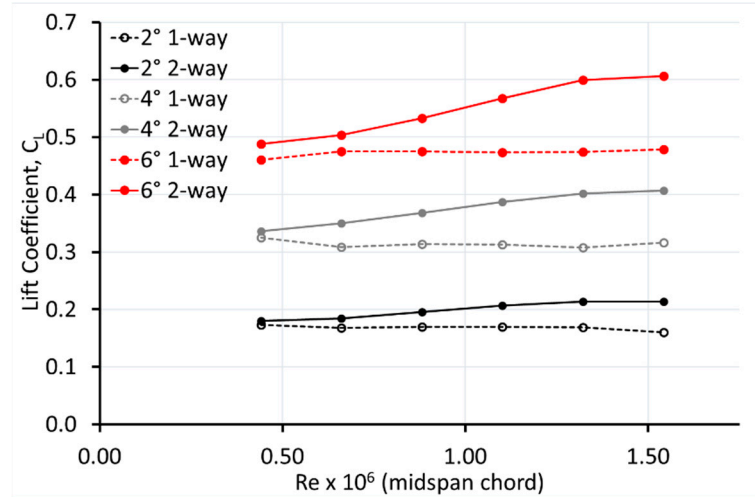


Figure 11. Lift coefficient vs. Reynold’s number.

However, for the two-way analysis, the lift coefficient increases with Reynold’s number (Figure 11). Again, the wash-in tip twist seen by the two-way analysis CFD (but not the one-way CFD) in Figure 8 could account for some of this increase in C_L , but again this figure and Figure 12 show that this does not fully explain the continuing increase in C_L as tip twist drops off at higher velocities.

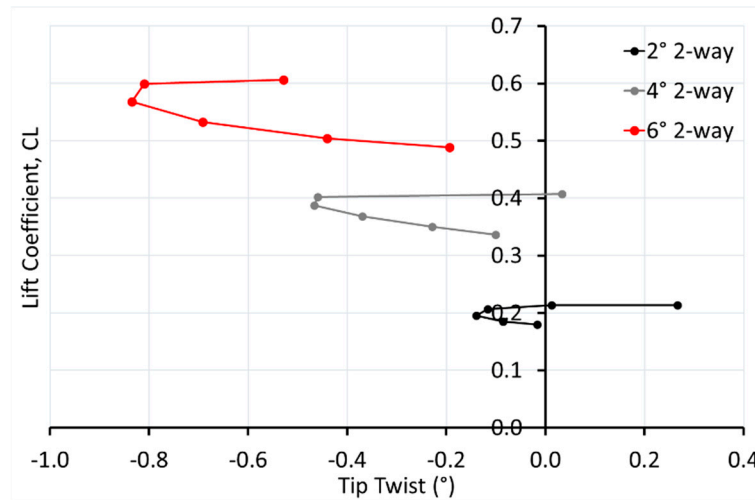


Figure 12. Lift coefficient vs. tip twist.

Figure 13 shows that, as expected, the variation of lift coefficient with AoA is linear in all cases for the sub-stall AoAs considered here. The one-way analysis (CFD loads assuming an un-deformed fin) gives an AoA lift slope (C_L/α) that is almost independent of velocity, and which is accurately predicted using the simple Prandtl equation:

$$\frac{C_L}{\alpha} = \frac{2\pi}{1 + \frac{2}{AR}} \tag{4}$$

where: α is in radians and AR is aspect ratio $sSpan^2/surface\ area = 37^2/300 = 4.56$

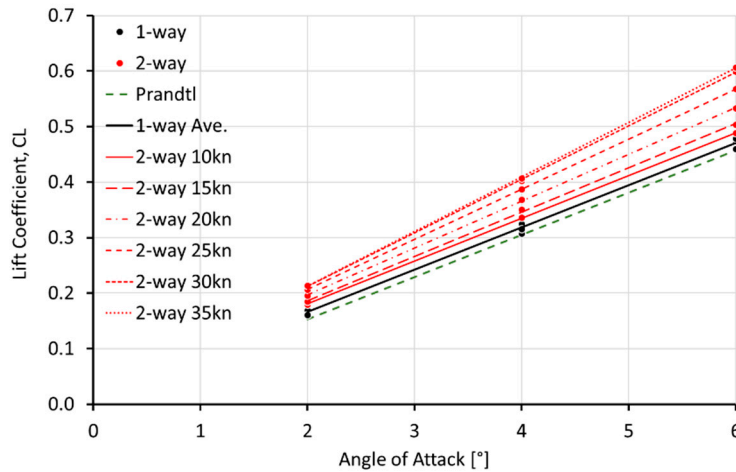


Figure 13. Lift coefficient vs. base chord AoA.

However, Figure 13 shows the two-way analysis lift slope increasing with velocity, as shown more clearly in Figure 14.

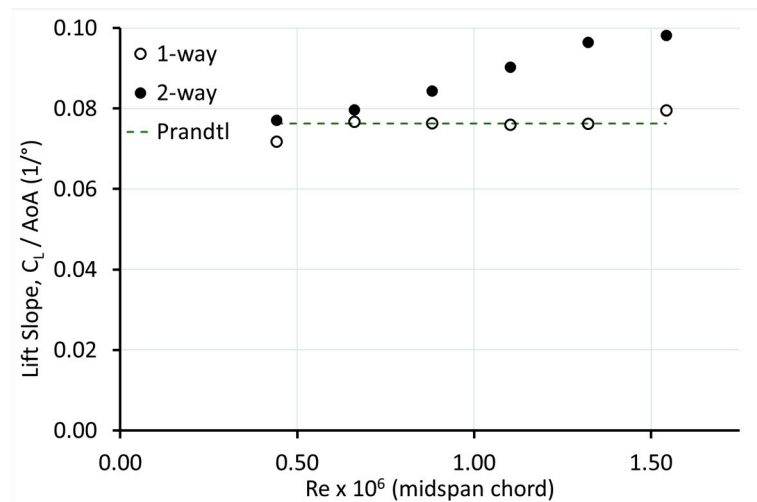


Figure 14. Lift slope vs. Reynold's number.

Replotting the tip twist data of Figure 8, as in Figure 15, shows that there is also a roughly linear increase in *wash-in* (negative twist angle) with angle of attack at each velocity, and that the slopes of this plot also increase with velocity.

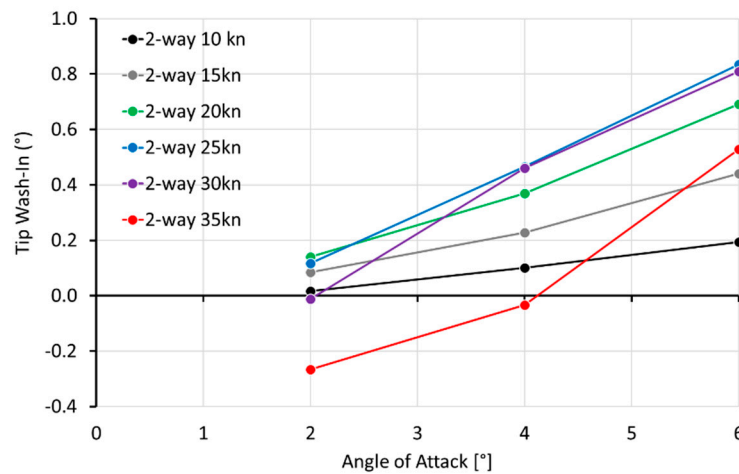


Figure 15. Tip wash-in (negative tip twist) vs. angle of attack.

Furthermore, plotting the 'wash-in slopes' of Figure 15 against the equivalent lift slopes of Figure 13 (and Figure 14), as in Figure 16, shows the strong correlation between the two, indicating some degree of causality.

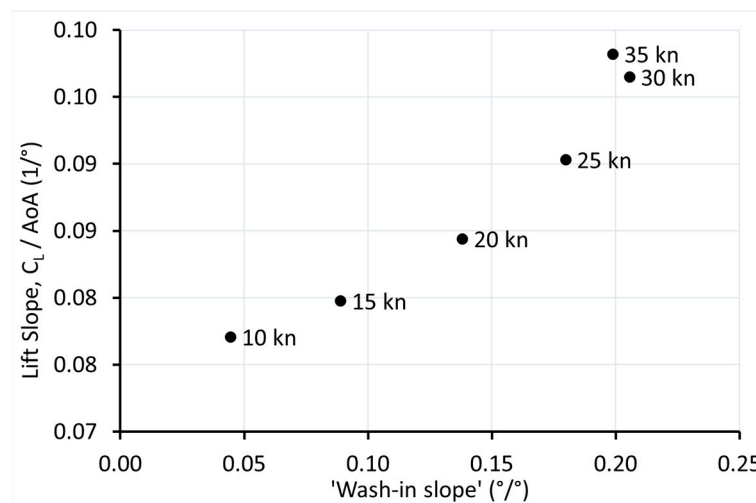


Figure 16. Lift slope-'wash-in slope' correlation.

The above discussion strongly indicates that the trends seen in the lift are in some way related to the variation in the tip twist, but identifying exactly which mechanism(s) are at play here requires further studies to be undertaken, since these mechanisms may well be complex and interacting. For example, although given the available data here this can only currently be hypothesised, the slightly reduced tip wash-in rotations seen at the highest velocities may reduce the tip vortex and hence increase lift. Further, investigation of the whole fin deformation (such as twist of the chord sections at various points along the span and any distortions leading to camber) is ongoing.

3.2.2. Drag

Drag force also increased with both velocity and AoA (Figure 7), as expected, but drag coefficient tended to decrease with velocity (Figure 17), which could be due to a reduction in skin friction drag (which dominates these streamlined chord sections) with increasing Reynold's number [32]. In addition, the pronounced drop in drag coefficient for both 6° AoA cases at a Reynold's number of around 1 million is typical of a reduction in the form drag component (which would be more significant at this higher AoA) as flow becomes more turbulent and hence boundary layer separation is hence delayed [33].

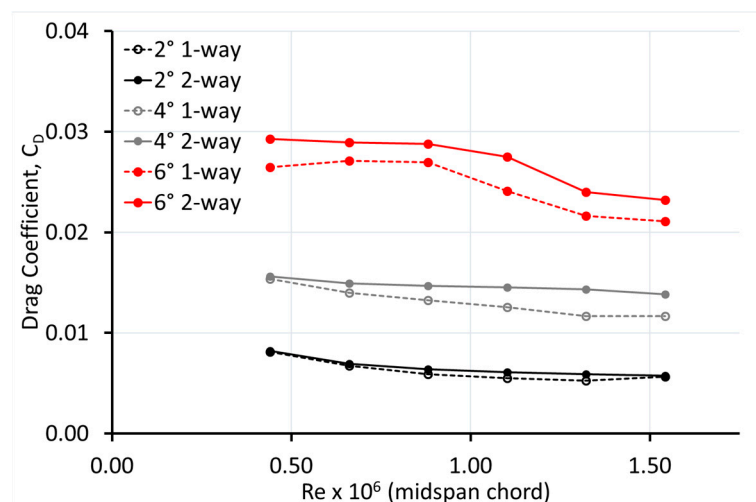


Figure 17. Drag coefficient vs. Reynold's number.

Except for the lowest velocity and AoAs of 2 and 4°, the two-way drag coefficient is consistently higher than that of the one-way analysis. As was seen for lift forces, this

could again be due to the higher tip angles of attack (wash-in) seen by two-way (but not the one-way) analysis, but again there does not seem to be a simple correlation between C_D and tip twist angle (Figure 18). Again, further study is required to investigate the physical mechanism(s) behind this behaviour, which may be complex and interacting.

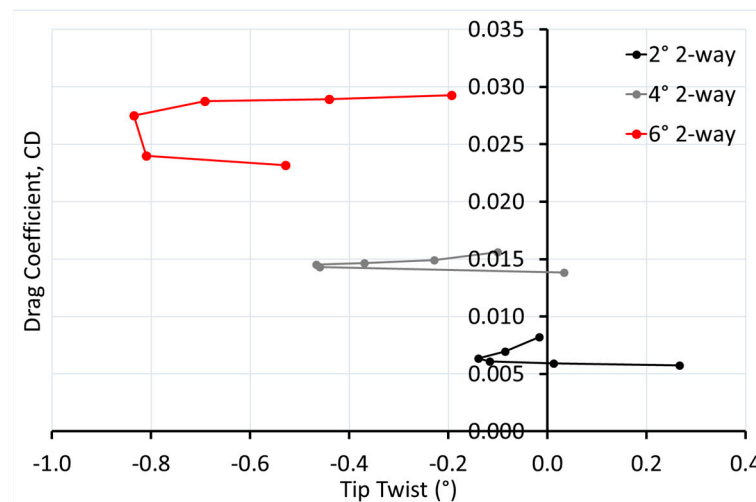


Figure 18. Drag coefficient vs. tip twist angle.

3.2.3. Tip Twist

Here, it must be noted that the current FEA model has been developed using continuum shell elements and validated experimentally under cantilever bending and that further work is underway to use recent experimental twist results to evaluate a modified FEA using solid elements. However, as will be discussed in Section 4, current results appear to mirror those obtained by previous studies.

For the one-way analysis, wash-in (negative twist) increases with both velocity and AoA (Figure 8). The two-way analysis also gives more wash-in at higher AoA at all velocities, but these values are lower than the one-way analysis predictions in all cases. As mentioned in the previous sections, for each AoA, as velocity increases the two-way wash-in increases, maximises and then decreases, even becoming wash-out (positive twist, reduced local AoA) for 2° AoA at 35 kn.

This tip twist may be due to two distinct mechanisms:

1. Hydrodynamic torsional moments between the section shear centre [34,35] and the centre of pressure
2. Structural bend-twist coupling due to planform sweep and/or laminate layup (see Section 4)

Both effects will vary along the span due to the (stepwise) varying lay-up and local AoA (from twist and/or finite wing effects), and are also likely to interact, leading to an extremely complex problem to solve, or even interpret, analytically. However, the two-way FSI analysis solves this problem numerically, predicting the behaviour shown in Figure 8.

Nevertheless, it is possible to gain some insight into the origins of the twist behaviour seen:

- (i) The main UD carbon stiffening plies are shown as darker shaded areas in Figure 2, indicating that the structural shear centre is significantly aft of the $\frac{1}{4}$ -chord line of the fin for the majority of its span. Since the fin foil section is symmetrical, the centre of pressure will be fairly close to the $\frac{1}{4}$ chord (for most of the span), leading to an overall hydrodynamic wash-in (negative twist, AoA increase) moment. However, at the tip, finite wing effects may produce a local hydrodynamic wash-out (positive twist, AoA decrease) moment [36].
- (ii) The aft-swept fin planform (due to the aft-swept leading edge) produces a wash-out (positive twist, AoA decrease) bend-twist coupling effect [3,34]. The symmetric,

balanced layup of nominally 0° UD and $\pm 45^\circ$ biaxial reinforcements theoretically gives no bend-twist coupling. However, since the plies are laid up with respect to the trailing edge, the plies are angled slightly forward with respect to the $\frac{1}{4}$ chord line and hence some degree of laminate induced wash-out (positive twist, AoA decrease) bend-twist coupling is also possible.

It is not possible from the data available to quantify the various torsional effects described above, but some useful qualitative deductions may be made:

- Hydrodynamic wash-in effects appear to be dominant, except at high velocity and lower AoA combinations (Figure 8).
- Since one-way and two-way tip deflections are similar (Figure 9), it can be deduced that the decrease in wash-in at higher velocities seen for the two-way analysis, but not for the one-way analysis, is not due to structural bend-twist coupling, and thus hydrodynamic wash-out moment effects appear to be responsible.
- The hydrodynamic loading from the rigid fin shape deforms the fin in such a way that the hydrodynamic tip torsional loadings are reduced (Figure 19).

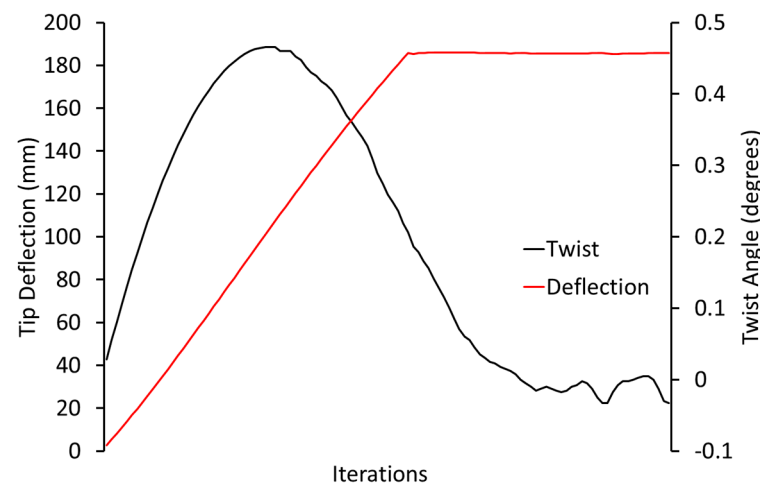


Figure 19. Evolution of tip twist and deflection with two-way iteration (4° AoA and 35 kn).

3.2.4. Tip Deflection

Tip deflection increases with velocity and AoA (and hence lift forces) in all cases, as expected (Figure 9). Deflections are also slightly higher for the two-way than for the one-way analysis. As discussed in Section 3.2.1, the tip wash-in seen for the two-way analysis but not for the one-way analysis would increase tip lift forces, and hence tip deflections. However, again, Figure 20 shows that there is no simple correlation between tip deflection and twist. Again, further work is required to investigate the mechanisms(s) responsible for these trends.

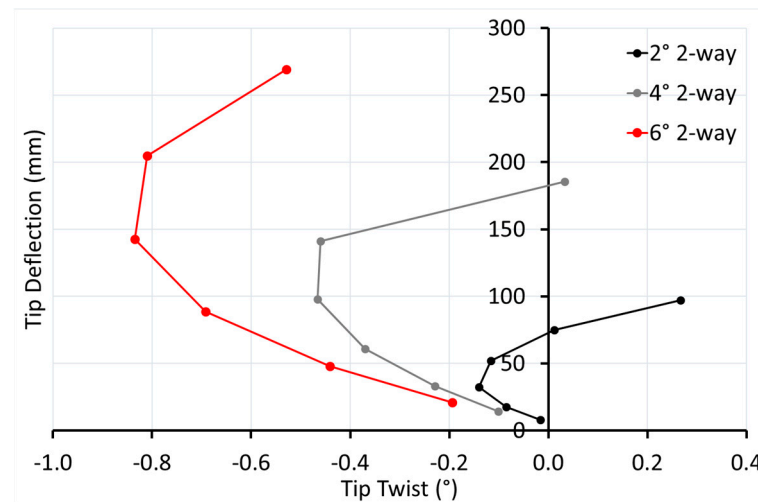


Figure 20. Tip deflection vs. tip twist (negative = wash-in = increased AoA).

4. Passive Tip Control

As discussed in the introduction, building a twist response into the fin gives the sailor better control in challenging conditions, but since this is achieved via a raked-back plan-form it results in non-optimal lift to drag ratios (i.e., control comes at the expense of speed). However, as described in Section 3.2.3, the non-homogenous internal structure of fibre composites allows tailoring of the material itself to give bend-twist coupling, i.e., pure bending loading produces twist (and vice versa). This allows for the possibility of retaining a fin planform for minimum drag (i.e., without resorting to rake) whilst causing the fin to ‘twist-off’ (i.e., reduce the AoA, ‘feather’ or ‘wash-out’) as it bends longitudinally at higher loadings to give better control—‘the best of both worlds’. Alternatively, if a fin already has too much wash-out then the bend-twist coupling can be modified to give less wash-out or even ‘wash-in’ (where longitudinal bending increases the AoA), increasing the ‘lift’ (in this case side force) produced by the fin.

Bend–twist coupling can be achieved in a laminated fibre composite by simply specifying a ‘symmetric’ layup—that is the plies above the mid-plane are a mirror image (in terms of fibre material, architecture, areal weights and fibre direction) of those below the mid-plane [37]. For example, by ‘rotating’ the fibres in the laminate of the upper and lower faces of a simple UD fibre composite box cantilever *in the same direction* as shown in Figure 21 (adapted from Figure 3 in [38]), bend twist coupling is obtained *in the sense shown*. Details of the laminate theory behind fibre composite bend–twist coupling is detailed in [37–43].

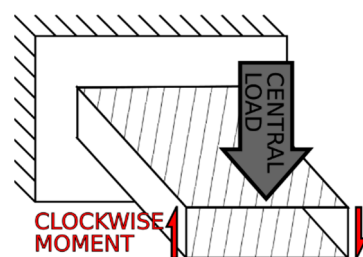


Figure 21. Bend-twist coupling.

This approach has already been successfully used in aerospace (originated by Krone [44] and famously successfully utilized for the forward swept wings of the Grumman X-29 experimental aircraft [45,46]), wind energy [38,43,47–52], tidal energy [53,54], composite marine propellers [55–61] and International Moth ‘foiling’ dinghy and larger surface-piercing sailing hydrofoils [62–69]. Much as for the X-29, the approach of Giovannetti et al. was to produce

bend-twist coupling by rotating the ply alignment symmetrically on the top and bottom surface of a supporting ‘wing box’ beam (c.f. Figure 21) embedded within the foil itself.

However, in this study, plies within the monolithic foil laminate itself are rotated to provide an integral solution. In Figure 22 the directions of the ply rotations required (symmetrically, on both leeward and windward faces of the fin) for longitudinal fin bending to produce wash-in (where twist increases the AoA) and wash-out (where twist decreases the AoA) are shown.

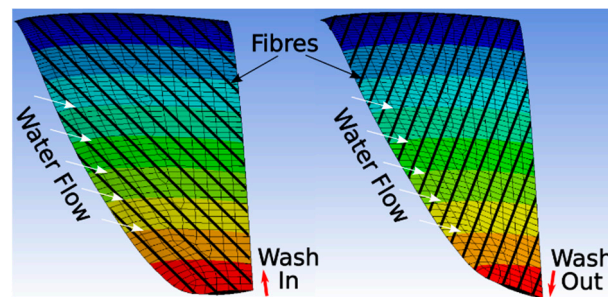


Figure 22. Fibre alignment for wash-in and wash-out (pressure, i.e., leeward side).

The influence of rotations of the full-face outer plies, 2 and 3, and 4 and 5, as those with most influence on the fin twist due to their distance from the fin centreline, on tip twist was investigated. Fibre rotation was defined here as positive for aft ‘rake’ since this is already a standard industry term used to describe the fin planform. Similarly, tip twist was defined with wash-out angle as positive (and hence wash-in as negative) since wash-out of sails generally is referred to as ‘twist’ or ‘twisting off’, and the fin is analogous, and indeed the exact counterpart, to the sail. These definitions make explanations of the scientific findings more easily digested by the windsurfing industry and wider community.

The previously developed FSI model is now used as a tool to explore this ‘hydro-elastic tailoring’ to try to achieve passive tip twist and deflection control, which constitute the two main fin characteristics affecting the ‘on the water’ sailing performance. Plies 2 and 3 were rotated together, aft and forward (up to 45° since these are balanced woven reinforcements with the same warp and weft fibres), and the obtained corresponding tip deflection and twist changes from that of the actual production fin layout are plotted in Figure 23.

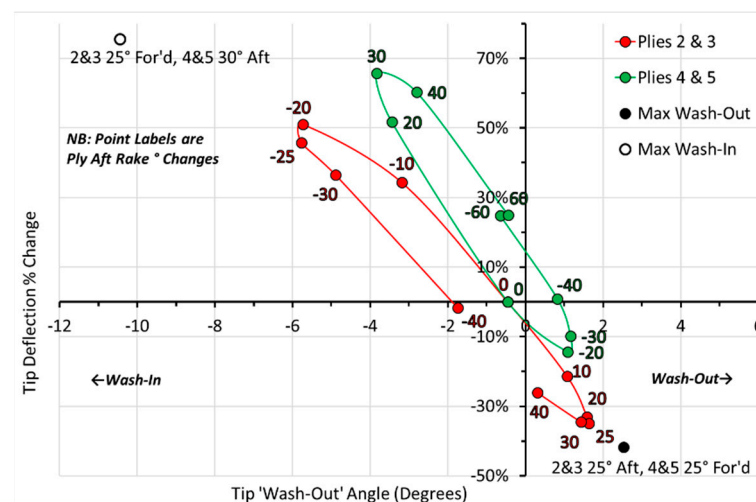


Figure 23. Two-way FSI variation of tip deflection and twist with ply rotation angles.

UD plies 4 and 5 were then rotated together to give the corresponding plot also shown in Figure 23. The required rotations for plies 2 and 3, and for 4 and 5, to give maximum wash-in were identified as 25° forward and 30°, respectively, and for maximum wash-out

25° forward and aft, respectively. Although the current FEA model uses shell elements and validation has been via experimental bending tests, these maximum and minimum twist angles of approximately 25° in Figure 23 (and Figures 24 and 25) correspond to those found in the literature [37,38]. Finally, the appropriate rotations were applied to all four plies 2 to 5, to give the maximum wash-out and wash-in points indicated in Figure 23.

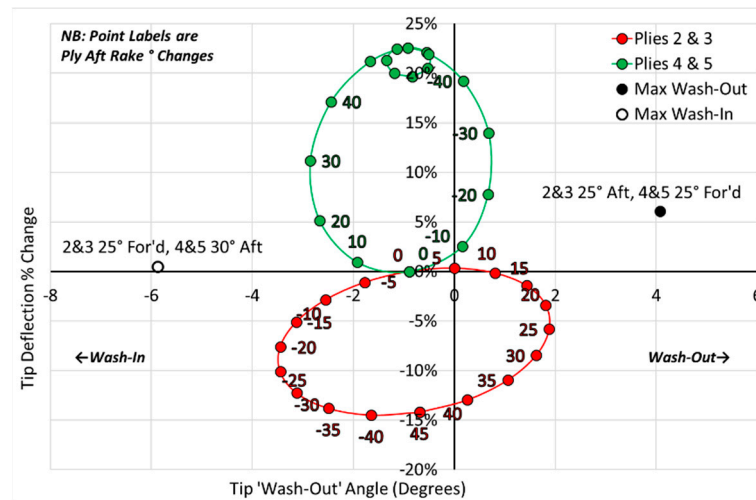


Figure 24. One-way FSI variation of tip deflection and twist with ply angles.

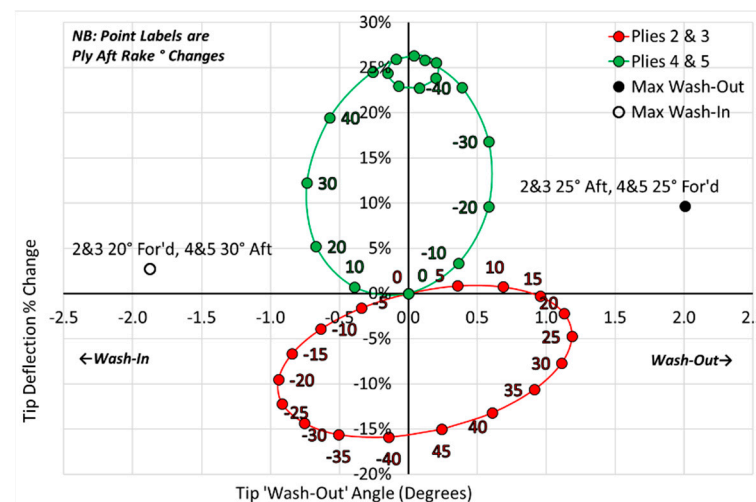


Figure 25. Simple point load variation of tip deflection and twist with ply angles.

Rotations of these plies appear to lead to very significant changes in tip twist, especially considering that these fins stall at AoAs of approximately 6 to 8°, and are operating (in theoretical ‘steady state’ sailing at least) at far lower AoAs. In terms of practical application of this work, the amount of wash-in or wash-out which will be ‘better’ is extremely difficult to define, and will no doubt depend on many variables such as wind and sea conditions, type of sailing competition, sailor weight, height and sailing style, sail type and size, etc. Furthermore, increases in tip wash-in and wash-out are accompanied here by increases and decreases in the tip deflection, respectively.

In fact, the only way to effectively identify an optimum bend-twist coupling response is to fabricate identical fins with maximum and minimum wash-out and wash-in and then allow on-the-water testing by professional, world-class sailors, which is currently underway. This should allow ‘translation’ (i.e., ‘calibration’) of the language of the test sailors’ reports (which are in terms of subjective terminology such as ‘control’, ‘speed’,

‘softness’, ‘ease of planning’, etc.) into what is actually happening to the fin hidden in the water under the board in terms of deflection and twist, which is the main aim of this work.

Since resources for research are *extremely* low in the windsurfing fin industry, putting full two-way FSI out of reach as a practical tool (that must be fully updated as fin forms and layups rapidly evolve and change), the effects of the ply rotations discussed above were investigated using the simpler, and hence more economical, one-way FSI analysis (Figure 24).

Figure 24, shows that, although the values differ, exactly the same conclusions would have been made using this plot as would have been made using the far more resource intensive full two-way FSI approach of Figure 23.

Further, since most, if not all fin producers have no access to full 3D CFD, nor FEA, and almost certainly not to full two-way FSI analyses, but could far more easily replicate the simple point loaded cantilever physical, mechanical type of test of Section 2.1.3, the FEA model was used to predict if this simple loading condition could be used to identify the ply rotations required for the different combinations of tip twist and deflection identified by the full two-way FSI. Figure 25 again shows that although the amounts of twist and deflections differ, the same conclusions would have been made using this plot as would have been made using the full two-way FSI approach of Figure 23. This is a very important finding as it indicates that simple mechanical cantilever tests can be used to identify the probable twist and deflection trends obtained via rotation of the outer plies that should be seen under actual sailing conditions, further helping this process of ‘translation’ of test sailor’s reports into fin deformations and hence to the laminators lay-up schedule.

5. Conclusions

A two-way full fluid-structure interaction (FSI) tool has been developed for a carbon and glass fibre reinforced composite windsurfer fin. An ABAQUS FEA verified against mechanical tests on an actual fin, was coupled with a STAR-CCM+ CFD model to give a fully iterative hydro-elastic solution. Composite laminate property data were developed, taking into account the actual production processes used. The FSI tool was then used to investigate the forces produced by, and deflections of, the fin under a range of typical sailing conditions, represented by combinations of two main parameters: velocity and angle of attack (AoA). Finally, the tool was used to investigate the effects on tip twist and deflection of ‘hydro-elastically tailoring’ the fin’s internal reinforcement layup specifications. The main conclusions of this work are:

A full two-way FSI analysis (which takes into account the CFD effects of fin deformations) gives better insights into the fin behaviour than does a one-way analysis (where CFD assumes a fully rigid fin), hence leading to different conclusions:

- The two-way FSI predicted more ‘lift’ force than did the simple one-way analysis.
- The one-way analysis and the Prandtl equation gave very similar predictions of ‘lift’ coefficient for all velocities, whereas the full two-way FSI predicted increasing lift coefficient and slope with Reynolds number.
- Both approaches predicted a decreasing drag coefficient with increasing Reynolds number, but the two-way FSI value was lower than that of the one-way analysis.
- The one-way analysis FSI predicted tip wash-in that increased both with AoA and velocity. The two-way FSI predicted significantly less tip wash-in, which decreased at higher velocities and even switched to wash-out at lower AoAs.
- Tip deflections were slightly higher for the two-way FSI than for the one-way analysis.

Hydrodynamic wash-in effects appear to be mainly dominant (except for lower AoAs at high velocities) and the hydrodynamic loading deforms the fin so that hydrodynamic tip torsional loadings are reduced.

Clearly, hydro-elastic tailoring of the fin laminate layup through simple ply rotations can lead to very significant changes in tip twist. This gives an opportunity for both passive control under highly loaded conditions and regulation of tip twist for higher speeds, both of which may be achieved whilst retaining a hydrodynamically optimised plan shape.

Importantly, simple inexpensive cantilever tests appear to be sufficient to make qualitative comparisons between the ‘on-the-water’ responses of fins with different layouts.

Further work is underway to develop the FEA model using solid elements and experimental twist results for validation, but the current study has already indicated how the behaviour of the fin changes in terms of the main responses under the whole range of probable sailing conditions. The work has already indicated some counter-intuitive responses that require further investigation, and exploration of the physical mechanisms behind some of the behaviour seen is still to be completed.

Author Contributions: Conceptualization, L.S.S.; methodology, L.S.S. and M.C.d.B.; validation, L.S.S., M.C.d.B., J.M.C.P. and M.R.A.; formal analysis, L.S.S. and M.C.d.B.; investigation, M.C.d.B.; writing—original draft preparation, L.S.S.; writing—review and editing, L.S.S., M.C.d.B., J.M.C.P. and M.R.A.; visualization, L.S.S. and M.C.d.B.; supervision, L.S.S., J.M.C.P. and M.R.A.; project administration, L.S.S. All authors have read and agreed to the published version of the manuscript.

Funding: LS Sutherland was funded by the FCT (Fundação para a Ciência e Tecnologia), under the Transitional Standard with contract IST-ID/164/2018. M Arruda is partially supported by the FCT, under the Transitional Standard—DL57/2016/N3/UI/CERIS/CT/165/2018 and under the PhD scholarship SFRH/BD/109957/2015. JMC Pereira’s work was supported by Fundação para a Ciência e a Tecnologia (FCT) through IDMEC, under LAETA, Project UIDB/50022/2020.

Institutional Review Board Statement: Not available.

Informed Consent Statement: Not available.

Data Availability Statement: Not available.

Conflicts of Interest: The authors declare no conflict of interest.

References

1. Appeal, C.O. Windsurfing International Inc. v. Tabur Marine (Great Britain) Ltd. *Rep. Patent, Des. Trade Mark Cases* **1985**, *102*, 59–82. [CrossRef]
2. World Sailing Speed Record Council, 500 Metre Records. 2021. Available online: <https://www.sailspeedrecords.com/500-metre> (accessed on 12 April 2021).
3. Sutherland, L.S. Windsurfer Fin Hydrodynamics. Master’s Thesis, University of Southampton, UK, 1993.
4. Sutherland, L.S.; Wilson, P.A. Windsurfer Fin Hydrodynamics. In *Marine, Offshore and Ice Technology*; Computational Mechanics Publications; WIT Press: Southampton UK, 1994; pp. 51–58. [CrossRef]
5. Broers, C.; Chiu, T.W.; Pourzanjani, M.M.A.; Buckingham, D.J. Effects of Fin Geometry and Surface Finish on Sailboard Performance and Manoeuvrability. In *Manoeuvring Control Mar. Craft MCMC 92, Computational Mechanics Publications*; Wilson, P.A., Ed.; WIT Press: Southampton, UK, 1992; pp. 275–289.
6. Chiu, T.W.; van den Bersselaar, T.; Broers, C.; Buckingham, D.J. The Effects of Tip Flexibility on the Performance of a Blade-Type Windsurfer Fin. In *Manoeuvring Control Mar. Craft MCMC 92*; Computational Mechanics Publications; WIT Press: Southampton, UK, 1992; pp. 261–274.
7. Chiu, T.W.; Broers, C.; Walker, A.; Baller, C. An experimental study of the effects of deformable tip on the performance of fins and finite wings. In *Proceedings of the 23rd Fluid Dynamics, Plasmadynamics, and Lasers Conference, Orlando, FL, USA, 6–9 July 1993*; American Institute of Aeronautics and Astronautics: Reston, VA, USA, 1993. [CrossRef]
8. Fagg, S.; Velay, X. Simulating the operation of a novel variable camber hydrofoil. In *Proceedings of the 1996 IEEE Aerospace Applications Conference, Aspen, CO, USA, 10–10 February 1996*; Volume 3, pp. 261–271. [CrossRef]
9. Fagg, S.; Velay, X. The development of a novel composite material hydrofoil through advanced computational techniques. *WIT Trans. Eng. Sci.* **1996**, *10*, 11. Available online: <http://www.witpress.com/elibrary/wit-transactions-on-engineering-sciences/10/8836> (accessed on 29 March 2017).
10. Fagg, S. The Development of a Reversible and Finitely Variable Camber Windsurf Fin. Ph.D. Thesis, Bournemouth University, Poole, UK, 1997. Available online: <http://eprints.bournemouth.ac.uk/12235/> (accessed on 12 August 2022).
11. Kunoth, A.; Schlichtenmayer, M.; Schneider, C. Speed windsurfing: Modeling and numerics. *Int. J. Numer. Anal. Model.* **2007**, *4*, 548–558.
12. ABAQUS, Abaqus Unified FEA-3DEXPERIENCE R2018. 2018. Available online: www.3ds.com (accessed on 1 August 2022).
13. Robert McNeel & Associates. *Rhinoceros 3D*; Robert McNeel & Associates: Seattle, WA, USA, 2010.
14. Barbero, E.J. *Finite Element Analysis of Composite Materials Using Abaqus*; CRC Press; Taylor & Francis Group: Boca Raton, FL, USA, 2013.
15. *ABAQUS Analysis User’s Guide*; Dassault Systèmes Simulia Corp: Providence, RI, USA, 2013.
16. Smith, C.S. *Design of Marine Structures in Composite Materials*; Elsevier Ltd.: Barking, UK, 1990.
17. Sleight, S. *Modern Boat Building Materials*; Conway Maritime Press Ltd.: London, UK, 1985.

18. ANSYS© 2022 R1, ANSYS Inc.: Cannonsburg, PA, USA, 2020.
19. Shenoi, R.A.; Wellicome, J.F. West European Graduate Education Marine Technology. In *Composite Materials in Maritime Structures; Volume 1 Fundamental Aspects*; Cambridge University Press: Cambridge, UK; New York, NY, USA, 1993.
20. Chamis, C.C. Simplified Composite Micromechanics Equations for Hygral, Thermal and Mechanical Properties. In Proceedings of the Thirty-eighth Annual Conference of the Society of the Plastics Industry (SPI) Reinforced Plastics/Composites Institute, Houston, TX, USA, 7–11 February 1983; p. 19.
21. Chamis, C.C. *Mechanics of Composite Materials Past, Present, and Future*; NASA: Blacksburg, VA, USA, 1984; p. 41.
22. Vignoli, L.L.; Savi, M.A.; Pacheco, P.M.; Kalamkarov, A.L. Comparative analysis of micromechanical models for the elastic composite laminae. *Compos. Part B Eng.* **2019**, *174*, 106961. [[CrossRef](#)]
23. Roopa, T.; Murthy, H.N.; Sudarshan, K.; Nandagopan, O.; Kumar, A.; Krishna, M.; Angadi, G. Mechanical properties of vinyl ester/glass and polyester/glass composites fabricated by resin transfer molding and hand lay-up. *J. Vinyl Addit. Technol.* **2014**, *21*, 166–173. [[CrossRef](#)]
24. Abdelal, N.; Donaldson, S.L. Comparison of methods for the characterization of voids in glass fiber composites. *J. Compos. Mater.* **2017**, *52*, 487–501. [[CrossRef](#)]
25. Nascimento, F. Windsurf Fin- Numerical and Experimental Analysis of Ultimate Strength. Master's Thesis, Instituto Superior Técnico, Lisbon, Portugal, 2017.
26. Altmann, A.; Gesell, P.; Drechsler, K. Strength prediction of ply waviness in composite materials considering matrix dominated effects. *Compos. Struct.* **2015**, *127*, 51–59. [[CrossRef](#)]
27. Saldanha, A.R.Q. Hydrodynamic and Fluid-Structure Interaction analysis of a Windsurf Fin. Master's Thesis, Instituto Superior Técnico, Lisbon, Portugal, 2019.
28. Siemens. *Simcenter STAR-CCM+*; Siemens: Munich, Germany, 2018.
29. Wang, Z.; Wang, Y.; Zhuang, M. Improvement of the aerodynamic performance of vertical axis wind turbines with leading-edge serrations and helical blades using CFD and Taguchi method. *Energy Convers. Manag.* **2018**, *177*, 107–121. [[CrossRef](#)]
30. Nayar, K.G.; Sharqawy, M.H.; Banchik, L.D.; Lienhard, V.J.H. Thermophysical properties of seawater: A review and new correlations that include pressure dependence. *Desalination* **2016**, *390*, 1–24. [[CrossRef](#)]
31. *Siemens Star-CCM+ User Guide*; Siemens: Munich, Germany, 2018.
32. Abbott, I.H.; von Doenhoff, A.E. *Theory of Wing Sections, Including a Summary of Airfoil Data*; McGraw-Hill: New York, NY, USA, 1959.
33. Munson, B.R.; Okiishi, T.H.; Huebsch, W.W. *Fundamentals of Fluid Mechanics*, 6th ed.; J. Wiley & Sons: Hoboken, NJ, USA, 2009.
34. Stodieck, O.; Cooper, J.E.; Weaver, P. Interpretation of Bending/Torsion Coupling for Swept, Nonhomogenous Wings. *J. Aircr.* **2016**, *53*, 892–899. [[CrossRef](#)]
35. Tatham, R. Shear Centre, Flexural Centre and Flexural Axis: An Attempt to Clear up Current Confusion and Provide Definitions Differentiating Between the Three Terms. *Aircr. Eng. Aerosp. Technol.* **1951**, *23*, 209–210. [[CrossRef](#)]
36. McAlister, K.W.; Takahashi, R.K. *NACA 0015 Wing Pressure and Trailing Vortex Measurements, (n.d.) 142*; NASA: Washington, DC, USA, 1991.
37. Ong, C.-H.; Tsai, S.W. Design, Manufacture and Testing of A Bend-Twist D-Spar, Sandia National Laboratories. 1999. Available online: http://infoserve.sandia.gov/sand_doc/1999/991324.pdf (accessed on 23 March 2017).
38. Fedorov, V. Bend-Twist Coupling Effects in Wind Turbine Blades. Ph.D. Thesis, Technical University of Denmark, Lyngby, Denmark, 2012. Available online: <https://core.ac.uk/reader/13803642> (accessed on 1 August 2022).
39. Barbero, E.J. *Introduction to Composite Materials Design*, 2nd ed.; CRC Press: Boca Raton, FL, USA, 2011.
40. Strong, A.B. *Fundamentals of Composites Manufacturing: Materials, Methods and Applications*, 2nd ed.; Society of Manufacturing Engineers: Dearborn, MI, USA, 2008.
41. Jones, R. *Mechanics of Composite Materials*, 2nd ed.; Taylor & Francis: Philadelphia, PA, USA, 1999.
42. Caprino, G.; Visconti, I.C. A Note on Specially Orthotropic Laminates. *J. Compos. Mater.* **1982**, *16*, 395–399. [[CrossRef](#)]
43. Fedorov, V.A.; Dimitrov, N.; Berggreen, C.; Krenk, S.; Branner, K.; Berring, P. *Investigation of Structural Behavior due to Bend-Twist Couplings in Wind Turbine Blades*; NAFEMS NORDIC Seminar: Esbjerg, Denmark, 2010.
44. Krone, N., Jr. Divergence elimination with advanced composites. In Proceedings of the Aircraft Systems and Technology Meeting, Los Angeles, CA, USA, 4–7 August 1975; American Institute of Aeronautics and Astronautics: Los Angeles, CA, USA, 1975. [[CrossRef](#)]
45. Johnsen, F.A. *Sweeping Forward: Developing & Flight Testing the Grumman X-29A Forward Swept Wing Research Aircraft*; National Aeronautics and Space Administration; Aeronautics Research Mission Directorate: Washington, DC, USA, 2013.
46. Wansack, J.K. *X-29 Advanced Technology Demonstrator Technical Activity Report*; USAF Flight Dynamics Laboratory: Wright-Patterson Air Force Base, OH, USA, 1983.
47. Kooijman, H.J.T. *Bending-Torsion Coupling of a Wind Turbine Rotor Blade*; ECN: Amsterdam, The Netherlands, 1996; Available online: <https://www.ecn.nl/publications/ECN-I-96-060> (accessed on 1 August 2022).
48. de Goeij, W.; van Tooren, M.; Beukers, A. Implementation of bending-torsion coupling in the design of a wind-turbine rotor-blade. *Appl. Energy* **1999**, *63*, 191–207. [[CrossRef](#)]
49. Lobitz, D.W.; Veers, P.; Eisler, G.R.; Laino, D.J.; Miglior, P.G.; Bir, G. *The Use of Twist-Coupled Blades to Enhance the Performance of Horizontal Axis Wind Turbines*; Sandia Report No. SAND2001-1303; Sandia National Labs: Albuquerque, NM, USA, 2001.

50. Lobitz, D.W.; Veers, P.S. Load Mitigation with Bending/Twist-coupled Blades on Rotors using Modern Control Strategies. *Wind Energy* **2002**, *6*, 105–117. [[CrossRef](#)]
51. Capellaro, M. Design Challenges for Bend Twist Coupled Blades for Wind Turbines: And Application to Standard Blades. 2012. Available online: <http://energy.sandia.gov/wp-content/gallery/uploads/2B-B-1-Capellaro1.pdf> (accessed on 23 March 2017).
52. Sompong, N. Effects of bend-twist coupling deformation on the aerodynamic performance of a wind turbine blade. *Int. J. Geomate*. **2017**, *12*, 15–20. [[CrossRef](#)]
53. Nicholls-Lee, R.; Turnock, S.; Boyd, S. Application of bend-twist coupled blades for horizontal axis tidal turbines. *Renew. Energy* **2012**, *50*, 541–550. [[CrossRef](#)]
54. Nicholls-Lee, R.F.; Boyd, S.W.; Turnock, S.R. Development of high performance composite bend-twist coupled blades for a horizontal axis tidal turbine. In Proceedings of the ICCM17: 17th International Conference on Composite Materials, Edinburgh, UK, 27–31 July 2009; Available online: <http://eprints.soton.ac.uk/67325> (accessed on 23 March 2017).
55. Liu, Z.; Young, Y.L. Utilization of bend–twist coupling for performance enhancement of composite marine propellers. *J. Fluids Struct.* **2009**, *25*, 1102–1116. [[CrossRef](#)]
56. Young, Y. Fluid–structure interaction analysis of flexible composite marine propellers. *J. Fluids Struct.* **2008**, *24*, 799–818. [[CrossRef](#)]
57. Blasques, J.P.; Berggreen, C.; Andersen, P. Hydro-Elastic Tailoring and Optimization of a Composite Marine Propeller. In Proceedings of the 13. European Conference on Composite Materials: Composites for Sustainable Progress, Stockholm, Sweden, 2–5 June 2008; p. 10.
58. Lin, H.J.; Lai, W.M.; Kuo, Y.M. Effects of Stacking Sequence on Nonlinear Hydroelastic Behavior of Composite Propeller Blade. *J. Mech.* **2010**, *26*, 293–298. [[CrossRef](#)]
59. Mulcahy, N.L.; Prusty, G.; Gardiner, C.P. Hydroelastic tailoring of flexible composite propellers. *Ships Offshore Struct.* **2010**, *5*, 359–370. [[CrossRef](#)]
60. Ahmed, A.; Wei, L. Theoretical and experimental methods on bend-twist coupling and damping properties with the relationship to lay-up of the composite propeller marine: A review. *Int. J. Eng. Sci. Technol.* **2012**, *1*, 2907–2917.
61. Young, Y.L.; Garg, N.; Brandner, P.A.; Pearce, B.W.; Butler, D.; Clarke, D.; Phillips, A.W. Load-dependent bend-twist coupling effects on the steady-state hydroelastic response of composite hydrofoils. *Compos. Struct.* **2018**, *189*, 398–418. [[CrossRef](#)]
62. Giovannetti, L.M.; Banks, J.; Boyd, S.; Turnock, S.; Zingoni, A. Developing tools for assessing the fluid structure interaction of passive adaptive composite foils. In *Insights and Innovations in Structural Engineering, Mechanics and Computation*; Taylor & Francis Group: Oxfordshire, UK, 2016; pp. 586–591. [[CrossRef](#)]
63. Giovannetti, L.M.; Banks, J.; Ledri, M.; Boyd, S.; Turnock, S. Fluid structure interaction design development of passive adaptive composite international moth foil. In Proceedings of the International Conference on Innovation in High Performance Sailing Yachts 4th Edition, Lorient, France, 28–30 June 2017; Available online: <https://eprints.soton.ac.uk/412152/> (accessed on 1 August 2022).
64. Giovannetti, L.M. Fluid Structure Interaction Testing, Modelling and Development of Passive Adaptive Composite Foils. Ph.D. Thesis, University of Southampton, Southampton, UK, 2017. Available online: <https://eprints.soton.ac.uk/412651/> (accessed on 1 August 2022).
65. Giovannetti, L.M.; Banks, J.; Ledri, M.; Turnock, S.; Boyd, S. Toward the development of a hydrofoil tailored to passively reduce its lift response to fluid load. *Ocean Eng.* **2018**, *167*, 1–10. [[CrossRef](#)]
66. Temtching, V.; Augier, B.; Dalmas, T.; Fagherazzi, O.; Dumergue, N. Analysis of Composite Layup Impact on Hydrodynamic Performances of Sail Yacht Flexible Hydrofoils. In Proceedings of the JH2018—16th Journées de l’Hydrodynamique, Marseille, France, 27–29 November 2018; p. 15.
67. Temtching, V.; Augier, B. Bend-Twist Coupling Analysis of Composite Hydrofoils with FSI. In Proceedings of the 24th Congr. Francais Mec., Brest, France, 26–30 August 2019.
68. Temtching, V.; Navale, E.; Augier, B.; Dalmas, T.; Dumergue, N.; Paillard, B. Impact of Composite Layup on Hydrodynamic Performances of a Surface Piercing Hydrofoil. In Proceedings of the 23rd Chesap. Sail. Yacht Symp., Annapolis, MD, USA, 15–16 March 2019; p. 15.
69. Vanilla, T.T.; Benoit, A.; Benoit, P. Hydro-elastic response of composite hydrofoil with FSI. *Ocean Eng.* **2021**, *221*, 108230. [[CrossRef](#)]